Citation for published version:
Cowper, P, Pockett, A, Kociok-Köhn, G, Cameron, PJ & Lewis, SE 2018, 'Azulene – Thiophene – Cyanoacrylic acid dyes with donor--acceptor structures. Synthesis, characterisation and evaluation in dye-sensitized solar cells', Tetrahedron, vol. 74, no. 22, pp. 2775-2786. https://doi.org/10.1016/j.tet.2018.04.043

DOI:
10.1016/j.tet.2018.04.043

Publication date:
2018

Document Version
Publisher's PDF, also known as Version of record

Link to publication

Publisher Rights
CC BY

University of Bath

General rights
Copyright and moral rights for the publications made accessible in the public portal are retained by the authors and/or other copyright owners and it is a condition of accessing publications that users recognise and abide by the legal requirements associated with these rights.

Take down policy
If you believe that this document breaches copyright please contact us providing details, and we will remove access to the work immediately and investigate your claim.

Download date: 22. May. 2019

Tetrahedron 74 (2018) 2775–2786

Contents lists available at ScienceDirect

Tetrahedron

journal homepage: www.elsevier.com/locate/tet

Azulene – Thiophene – Cyanoacrylic acid dyes with donor-π-acceptor structures. Synthesis, characterisation and evaluation in dye-sensitized solar cells

Paul Cowper [a, *], Adam Pockett [b], Gabriele Kociok-Köhn [c], Petra J. Cameron [a, b], Simon E. Lewis [a, b, *]

[a] Department of Chemistry, University of Bath, Bath, BA2 7AY, UK
[b] Centre for Doctoral Training in Sustainable Chemical Technologies, University of Bath, Bath, BA2 7AY, UK
[c] Chemical Characterization and Analysis Facility, University of Bath, Bath, BA2 7AY, UK

ARTICLE INFO

Article history:
Received 8 March 2018
Received in revised form
12 April 2018
Accepted 16 April 2018
Available online 17 April 2018

Keywords:
Azulene
Solar cell
DSSC
Sulfonium
Cross-coupling
Radical stabilization

ABSTRACT

We report the synthesis of five new azulene containing dyes, having D-π-A type structures. These dyes are synthesised using a sulfonium salt cross-coupling reaction. The dyes have been evaluated spectroscopically, electrochemically, crystallographically, and as sensitizers in dye-sensitized solar cells. We propose a rationale for the dyes' spectroscopic properties and performance in cells, based on conformational data derived from their crystal structures.

© 2018 The Authors. Published by Elsevier Ltd. This is an open access article under the CC BY license (http://creativecommons.org/licenses/by/4.0/).

1. Introduction

Since the earliest reports on dye-sensitized solar cells (DSSCs) over 25 years ago,[1,2] much effort has been expended in the optimisation of these devices, in pursuit of higher photoelectric conversion efficiencies (PCEs, η). Central to this effort has been the design, synthesis and evaluation of dyes with enhanced properties in terms of photon capture, electron injection, dye adhesion and device lifetimes, etc.[3,4] Dyes consisting of ruthenium polypyridyl complexes such as N719[5] achieved notably high PCEs, but the high cost of ruthenium is an impediment to the commercialisation of cells based on such dyes. In contrast, DSSCs that use wholly organic dye molecules can avoid the use of expensive metals. Design principles for high efficiency organic dyes have been established, with the donor–π linker–acceptor–anchor (D-π-A) assembly proving to be highly successful.[6,7] Of the various known electron donor motifs, arylamines have proven especially effective.[8–10] Regarding the π linker motif, a wide variety have been explored, mostly heterocycles, amongst which thiophenes, oligothiophenes and annulated thiophenes have all proven often to influence positively the overall cell efficiency.[11–16] An anchoring group is required to immobilise the dye molecule on the metal oxide surface; a variety of different anchor groups have been investigated, including phosphonic acids and carboxylic acids and their derivatives (esters, acid chlorides, carboxylate salts or amides).[17,18] Carboxylic acid and cyanoacrylic acid groups are most frequently used for DSSC dyes. More specifically, because of its excellent electron withdrawing characteristics, cyanoacrylic acid is used in most D-π-A organic dyes, where it fulfils the dual role of acceptor and anchor. In contrast, simple carboxylic acid anchors are usually used for transition metal complexes where metal-to-ligand-charge-transfer (MLCT) predominates.

The aims of the present study were to synthesise organic dyes for DSSCs that comprise an azulene ring as the donor motif, to characterise these dyes using a variety of techniques, and to evaluate their performance in solar cells. Azulene (**1**) is a bicyclic, nonbenzenoid aromatic hydrocarbon and is an isomer of

* Corresponding authors.
E-mail addresses: p.cowper@bath.ac.uk (P. Cowper), s.e.lewis@bath.ac.uk (S.E. Lewis).

https://doi.org/10.1016/j.tet.2018.04.043
0040-4020/© 2018 The Authors. Published by Elsevier Ltd. This is an open access article under the CC BY license (http://creativecommons.org/licenses/by/4.0/).

naphthalene (**2**). Azulenes have long been of interest to chemists due to their striking colours, interesting chemistry and unusual electronic properties. Azulene derivatives may be used as advanced materials for optoelectronic[19–25] and electrochromic[26] devices, charge-transport,[27–29] nonlinear optics[30] and chemical sensing[31]; some recent reviews serve to summarise these areas.[32,33] Some azulene derivatives have also been shown to have anti-inflammatory,[34,35] antiulcer,[36–38] anticancer[39–42] and anti-HIV[43] properties. Azulene is a non-alternant hydrocarbon, unlike naphthalene, which leads to HOMO nodes at C2 and C6 and LUMO (S_1) nodes at C1 and C3 (Fig. 1), causing relatively small repulsion between the electrons occupying these orbitals, meaning a low $S_0 - S_1$ transition energy, in the visible region.[44] With naphthalene **2**, the coefficient magnitude at different carbons is the same for the HOMO and LUMO, giving a higher degree of overlap, and the electrons occupy the same space with consequent higher repulsion and higher transition energy in the UV. Therefore naphthalene is colourless but azulene **1**, because the $S_0 - S_1$ transition corresponds to the green and red regions of the spectrum, is a deep blue colour. The absorption spectra for substituted azulenes are very sensitive to the electronic nature of the ring substituents.[45] Hence, by careful design of the substituents, the entire visible (and IR) spectrum is accessible. This ability to tune the chromophore's absorption spectrum makes azulene an attractive motif for exploitation in DSSCs.

In the context of solar cells, sporadic reports of azulene derivatives have appeared in various contexts. Emrick and co-workers employed copolymers of 2-substituted azulene with zwitterionic methacrylates in bulk-heterojunction (BHJ) solar cells.[46] Imahori and co-workers evaluated copolymers of 1,3-disubstituted azulene and diketopyrrolopyrroles or benzothiadiazoles[47] in BHJ solar cells, shortly after which and Liu, Zhang and co-workers reported two similar azulene copolymers, as well as a further example possessing distinct connectivity (a 4,7-disubstituted azulene).[48] Most recently, Gao and co-workers reported a copolymer incorporating a 6,6′-disubstituted 2,2′-biazulenyl.[49] Aside from polymer BHJ solar cells, Huang and co-workers recently reported the use of an azulene-squaraine small molecule in an organic photovoltaic (OPV) device.[50] Torres, Guldi and co-workers reported an OPV device comprising azulenocyanines immobilised on carbon nanotubes.[51] In the area of perovskite solar cells, an azulene-containing hole-transport material has been shown by Wakamiya, Saeki, Scott, Murata and co-workers to exhibit performance superior to that of Spiro-OMeTAD, the most commonly used hole-transport material.[52] There have been reports of electron injection from an azulene into the conduction band of titania, from Piotrowiak, Galoppini and co-workers[53,54] (either employing azulene itself, sequestered in a hemicarceplex, or using azulenes bearing methyl ester anchoring groups), but in no instance was construction of a DSSC attempted.

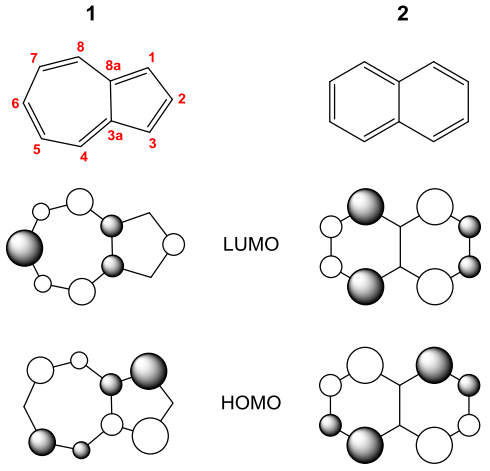

Fig. 1. Structures of azulene and naphthalene; their HOMOs and LUMOs.

To our knowledge, the peer-reviewed literature contains only two reports of azulene containing dyes being used in DSSCs. In 2007, Cheng, Wang, Zhang and co-workers reported the synthesis of dyes **3**–**6** (Fig. 2), comprising either an azulene attached directly to a cyanoacrylic acid (**3**, **5**), or with a vinylene linker between the azulene and the anchor motif (**4**, **6**).[55] They found the presence of the vinylene linker led to a bathochromic shift of λ_{max} and an increase in η with respect to the dyes lacking this motif, due to increases in both J_{SC} and V_{OC}. Additionally, they observed an increase in η for alkylated azulenes **5** and **6** compared to their respective non-alkylated counterparts **3** and **4**. The authors ascribe this latter effect to the alkyl groups disfavouring dye aggregation on the titania surface. In 2014, Hanaya and co-workers reported the evaluation of phenylazulene **7** (Fig. 2) as a dye in a DSSC.[56] The focus of this study was the evaluation of an alternative redox mediator, Br^-/Br_3^-, in place of the more commonly used I^-/I_3^- system, with the authors finding that the Br^-/Br_3^- system afforded a greater V_{OC} and hence η. The patent literature also contains azulene dyes for DSSCs. Two patents filed by TDK[57,58] describe azulenes **8**–**17** (Fig. 2). The emphasis of the patent is on the fact that these dyes are all more resistant to photobleaching than a comparator ruthenium-based dye; no further data are given. A patent from Solvay[59] reports azulenocyanines of type **18** (Fig. 2), which differ from those reported previously by Torres, Guldi and co-workers[51] in that the azulenocyanines bear anchoring groups for the specific purpose of attachment to titania and use in a DSSC. (Azulenes are also described elsewhere in the patent literature in the broader context of photovoltaics.[60,61]) Finally it should be noted that prospective azulene-based dyes for DSSCs have been considered theoretically.[62]

2. Results and discussion

In the present study, we undertook two rounds of dye design, synthesis and characterisation. In the first instance we targeted dyes of the D-π-A design, with a 1-substituted azulene as the donor motif (as per the majority of examples in Fig. 2), and a cyanoacrylic acid as the acceptor and anchor motif. For the π-linker, we opted to employ a thiophene ring, whose ability to induce bathochromic shifts of absorption maxima and to afford increased extinction coefficients has been documented.[11–16] Specifically we targeted azulene-thiophene-cyanoacrylic acid ("Az-tcaa") **19** and 4,6,8-trimethylazulene-thiophene-cyanoacrylic acid ("TMAz-tcaa") **20** (Fig. 3). The rationale for targeting **20** was that the methyl substituents may disfavour dye aggregation on the titania surface, analogous with the reason proposed previously[55] for the increased performance of **6** with respect to **4**. Retrosynthetically, it was envisaged that the targets could be accessed by a Knoevenagel condensation of aldehyde **22** and cyanoacetic acid. Aldehyde **22** would be accessed in turn using cross-coupling methodology, from an appropriately functionalised azulene **23** and a thiophene-2-carbaldehyde metallated at the 5-position, **24**. The C1 and C3 positions of azulene are the most nucleophilic, so a haloazulene of type **23** would be expected to be accessible from the parent azulene (**1** or **25**) through an S_EAr halogenation.

Of the various cross-coupling methodologies that could be used to synthesise **22**, we opted to employ a Suzuki–Miyaura reaction, since there is precedent for such couplings using 1-haloazulenes as the substrate,[63] in conjunction with bulky monodentate phosphine

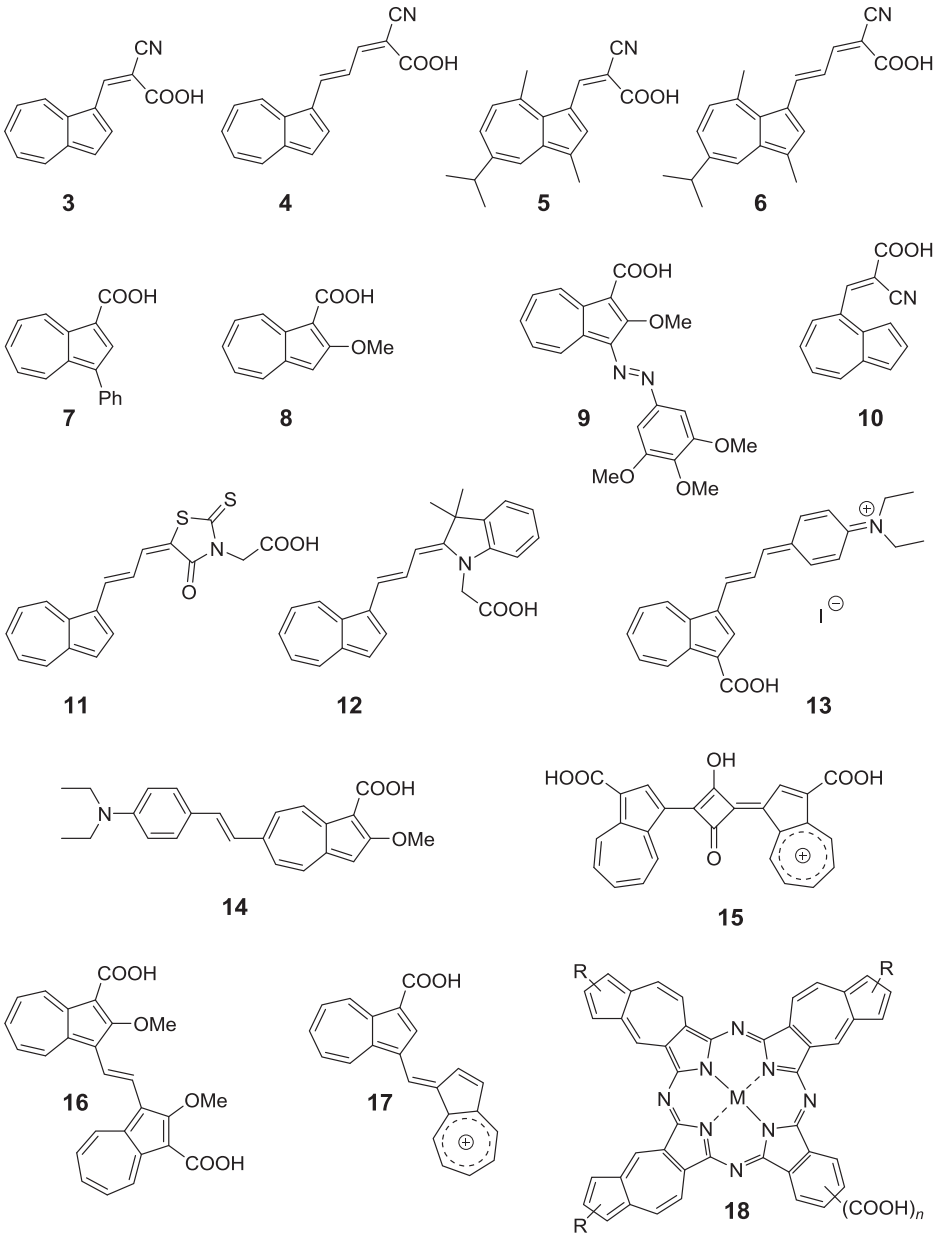

Fig. 2. Previously reported azulene-containing dyes used in DSSCs.

ligands.[64] The required nucleophilic reaction partner of type **24** was therefore (5-formylthiophen-2-yl)boronic acid (**29**). This was synthesised through a variant of reported procedures,[65,66] as shown in Scheme 1a. We found that **29** could be conveniently purified by recrystallization from water, although the polymorph so formed was shown by x-ray crystallography to be a monohydrate (see ESI). This water of crystallisation could subsequently be removed simply by drying the ethereal solution of **29**•H_2O over $MgSO_4$.

An azulene cross-coupling partner was prepared by direct halogenation of azulene (**1**) with *N*-chlorosuccinimide to give 1-chloroazulene (**30**).[67] Clean monohalogenation of azulene through an S_EAr process is not possible, since the resultant 1-haloazulene can readily undergo a second substitution. Thus, even with only 1 equivalent of NCS, formation of a small quantity of 1,3-dichloroazulene (**31**) is unavoidable (Scheme 1b). Haloazulenes are also rather unstable, but **30** is sufficiently stable to be separable from **31** by chromatography. With both coupling partners in hand, we attempted their union using reaction conditions described by Buchwald.[64] In the first instance (Scheme 1c), however, thienyl azulene **32** was produced in only 6% yield. We ascribe this low yield primarily to instability of boronic acid **29** to the reaction conditions, as we observed significant quantities of protodeborylation product (thiophene-2-carbaldehyde) being formed. Decomposition of **30** may also have contributed to the low yield. Use of the bromo analogue of **30** was considered but not attempted, since although it would be more reactive, it is appreciably more unstable. Attempts at reaction optimisation (variation of solvent, reaction stoichiometry, etc.) afforded only marginal improvements in yield.

A significant improvement in the cross-coupling yield was achieved by varying the nucleophilic coupling partner, employing a pinacolborane group in place of the boronic acid, and with the aldehyde protected as an acetal. Thus, coupling of **30** with dioxaborolane **33** gave protected thienylazulene **34** (which was not purified); immediate deprotection by transketalisation in acetone

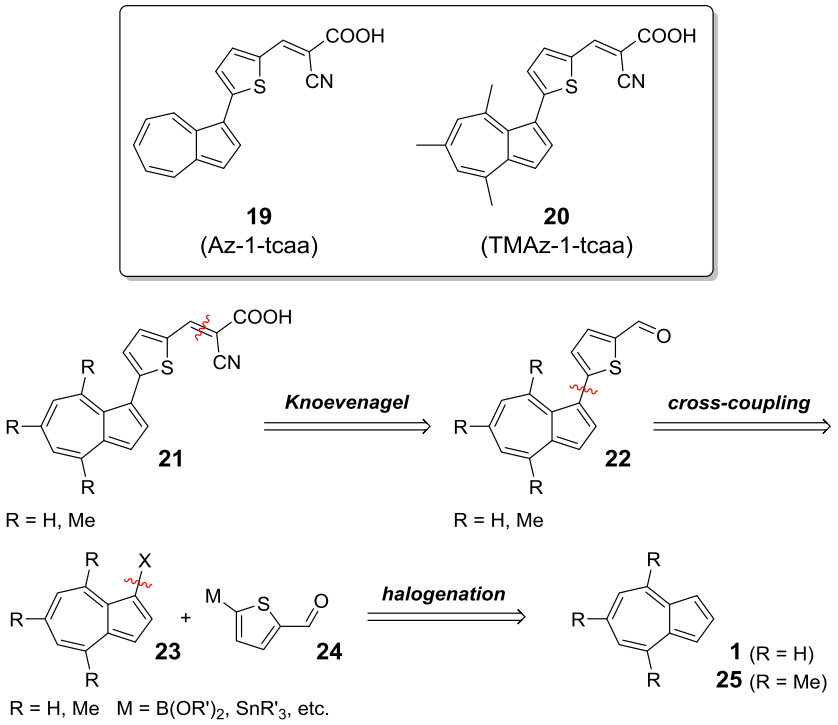

Fig. 3. Targeted 1st generation dyes and retrosynthesis.

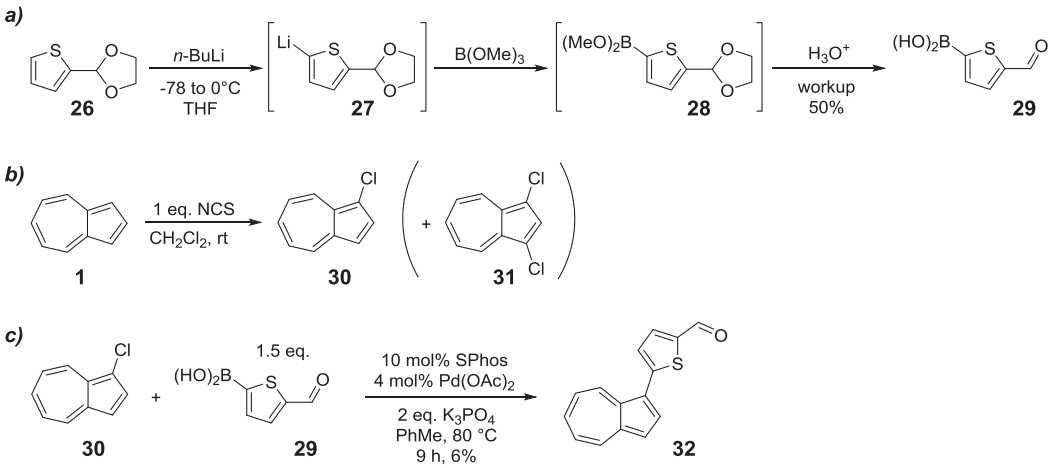

Scheme 1. Synthesis of cross-coupling partners and first Suzuki–Miyaura coupling.

gave desired aldehyde **32** in a much-improved 54% yield over 2 steps (Scheme 2a). The analogous reaction sequence with 4,6,8-trimethylazulenyl halide **35** gave the corresponding aldehyde **37** in 59% yield (Scheme 2b). Finally, the yields were improved still further by the use of azulenesulfonium salts **38**–**39** as pseudohalides in the cross-coupling (Scheme 2c), methodology recently developed by us to address the issue of the instability of azulenyl halides.[68]

With the required aldehydes **32** and **37** in hand, we carried out the Knoevenagel condensation to furnish the desired dyes **19** and **20** respectively, as shown in Scheme 3. Literature dye **3** was also synthesised[55,69] for spectroscopic comparison with **19**.

Absorption spectra for **3**, **19** and **20** were acquired in acetonitrile (see ESI), and key spectroscopic data are shown in Table 1. The spectra have similar features, such as an absorption in the 400–500 nm region, a region where corresponding the unsubstituted parent azulene compounds do not absorb. When comparing literature dye **3** with our dye **19** incorporating a thiophene π-linker, a bathochromic shift of λ_{max} of 50 nm is evident.

Cyclic voltammetry (CV) was then used to determine the oxidation potentials of the three azulene based dyes: Az-1-caa (**3**), Az-1-tcaa (**19**), and TMAz-1-tcaa (**20**) (Figs. 4–6). All CVs were run in dry THF with 0.1 M tetrabutylammonium hexafluorophosphate (Bu_4NPF_6) supporting electrolyte at a scan rate of 100 mV s^{-1} (see ESI for full details). Three scans were taken for each run. The voltammograms show plots for the first and third scans only. All the dyes exhibited at least one oxidation peak; however the oxidations were all irreversible so it was not possible to calculate the $E_{½}$ potentials. The peak oxidation potentials vs. Fc/Fc^+ are summarised below (Table 2). The position of the HOMO is estimated from the

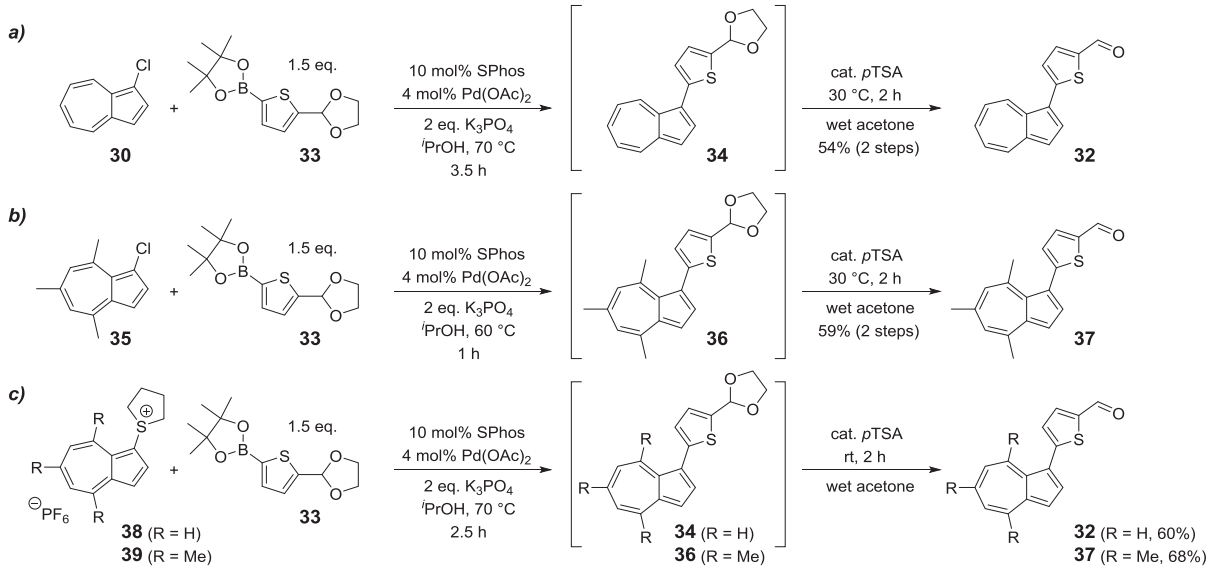

Scheme 2. Improvements to the cross-coupling.

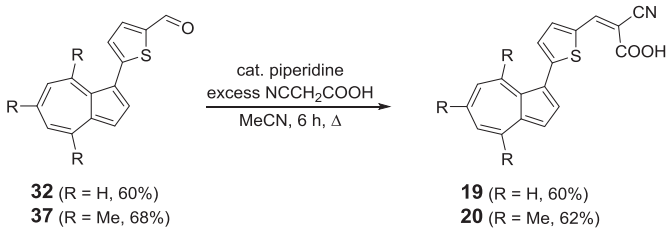

Scheme 3. Knoevenagel condensations.

Table 1
UV/Vis data for 1st generation dyes.

Dye	λ_{max} nm	ε L mol^{-1} cm^{-1}	λ_{onset} nm	E_g (opt) eV
Az-1-caa (**3**)	423	3.952×10^4	460	2.70
Az-1-tcaa (**19**)	473	3.026×10^4	547	2.27
TMAz-1-tcaa (**20**)	452	1.914×10^4	547	2.27

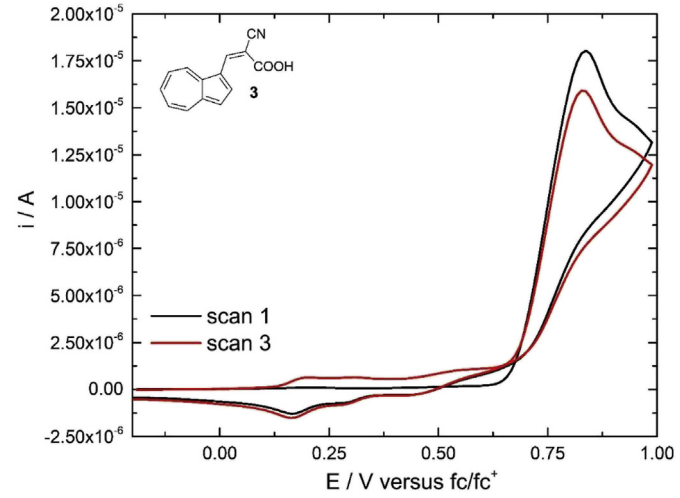

Fig. 4. Voltammogram for Az-1-caa (**3**), 0.5 mM in THF. Supporting electrolyte 0.1 M Bu_4NPF_6. Scan rate 100 mV s^{-1}.

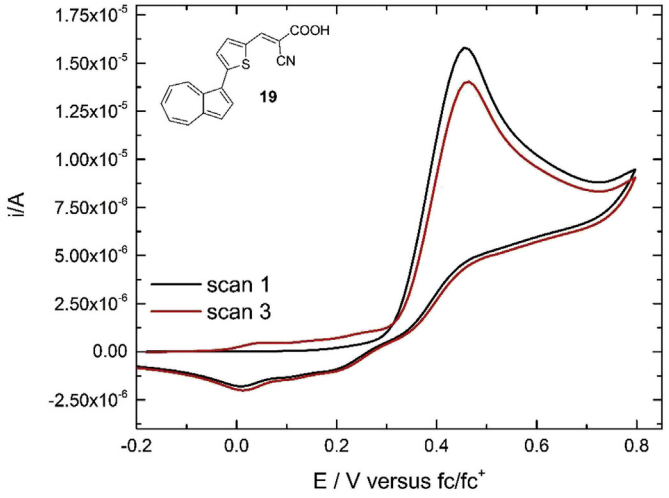

Fig. 5. Voltammogram for Az-1-tcaa (**19**), 0.5 mM in THF. Supporting electrolyte 0.1 M Bu_4NPF_6. Scan rate 100 mV s^{-1}.

onset of the oxidation wave in the irreversible scans.

The dye with three methyl groups on the azulene (**20**) has a similar oxidation potential to the unsubstituted analogue **19**. Furthermore, the literature dye without a thiophene linker (**3**) has a significantly elevated oxidation potential compared with the dyes with a thiophene linking unit (**19** and **20**). This suggests that the thiophene linker makes it easier to extract an electron from the dye molecule and that the resulting cation should be more stable. Also of note, **20** exhibited two oxidation waves, neither being reversible (Fig. 6). This means that two electrons can be removed from this molecule, resulting in a dication. Crucially, all of the voltammograms show that breakdown products are generated following oxidation of the dyes. This can be seen by comparing the traces of scan 1 (black line) and scan 3 (red line) in each voltammogram. With scan 1, there is no sign of any oxidation before the main oxidation peak begins, *e.g.* at approx. 0.3 V in Fig. 6. On subsequent scans, there is evidence of oxidation processes occurring at potentials lower than the main oxidation peak, *e.g.* in Fig. 6 two minor oxidation peaks can be seen at −0.049 V and 0.263 V vs Fc/Fc^+.

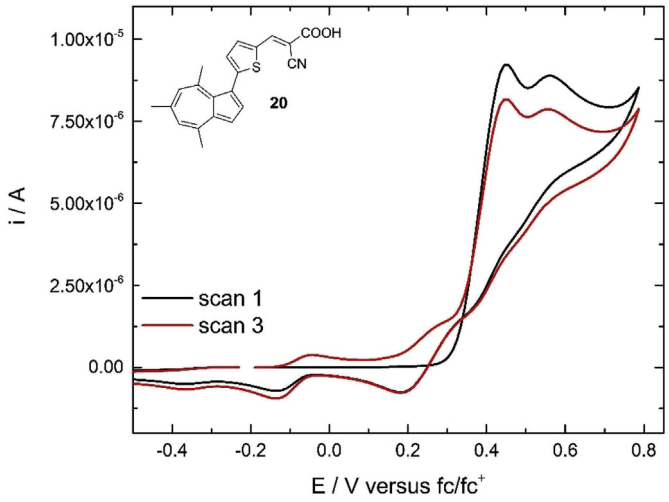

Fig. 6. Voltammogram for TMAz-1-tcaa (**20**), 0.5 mM in THF. Supporting electrolyte 0.1 M Bu_4NPF_6. Scan rate 100 mV s^{-1}.

These minor oxidation waves appear to be at least partially reversible since they have corresponding reduction waves. Since the minor oxidation waves did not occur in the first scan, they must be due to species generated from the oxidised dye, which is a radical cation. Such a radical cation would be highly reactive and may react with other molecules present *e.g.* solvent, other dye molecules (hydrogen abstraction) or other radicals (combination).

The cyclic voltammetry data discussed above suggest these dyes may have a limited lifetime in a DSSC. We were mindful of the fact that a characteristic of successful ruthenium polypyridyl dyes is that they are known to exhibit reversible electrochemistry.[70] Therefore, the objective of the second phase of this work was to synthesise dyes which exhibited reversible electrochemistry, which through modifications to Az-1-tcaa (**19**) and TMAz-1-tcaa (**20**) were rationally designed to stabilise their oxidised states.

A literature search for azulene-containing compounds with reported electrochemical data, and that exhibit reversible oxidation waves, has suggested that both the azulene C-1 and C-3 positions must be substituted, preferably with substituents with steric bulk *e.g. tert*-butyl groups. Gerson et al. have reported that only azulenyl radical cations substituted at both the C-1 and C-3 positions were sufficiently persistent to be characterised by EPR spectroscopy, and *tert*-butyl groups were necessary to enable ENDOR and TRIPLE resonance studies.[71] The radical cations of 1,3-di-*tert*-butylazulenes **40** (Fig. 7) persisted for 20–40 min at 273–283 K. The authors offered no explanation as to why the *tert*-butyl groups should confer stability to the azulene radical cation. 1,3-Dimethylazulene radical cations were more stable than those of unsubstituted azulene, but were not so long-lived as the 1,3-di-*tert*-butylazulene ones. It is postulated that the *tert*-butyl groups shield the radical unpaired electron purely through their steric bulk, preventing the close approach of species that would otherwise be liable to react with the radical. Shoji, Ito, Morita and co-workers have reported that 1,3-bis(methylthio)azulenes **41** also exhibit reversible

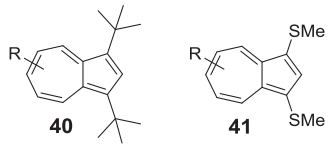

Fig. 7. Reported classes of azulenes exhibiting reversible electrochemistry.

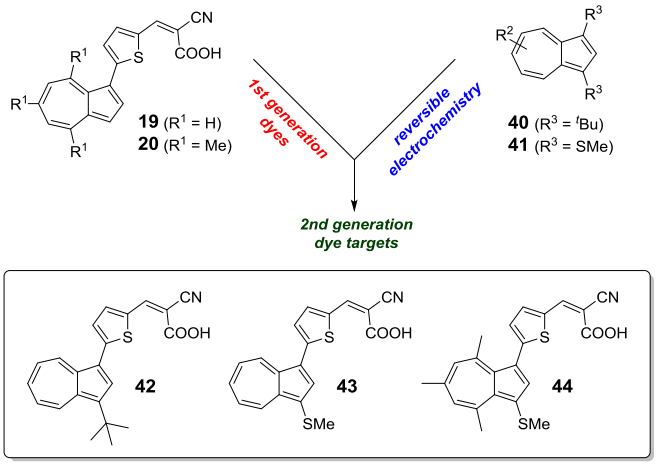

Fig. 8. Second generation azulene D-π-A dye targets.

electrochemistry.[72] The methylthio groups may also stabilise the corresponding radical cations through steric shielding; conjugation with the sulfur atoms may also be important.

We resynthesized 1,3-di-*tert*-butylazulene and 1,3-bis(methylthio)azulene and verified that they both do exhibit reversible electrochemistry (ESI, Figs. S4–S5). An azulenyl nitrone reported by Becker, Echegoyen and co-workers to exhibit reversible electrochemistry was also resynthesized.[73] While this did not display evidence of decomposition products, nor did it display fully reversible electrochemistry in our hands, as the amplitude of the oxidation wave decreased in the second and subsequent scans (ESI, Figs. S6–S7). These literature examples of azulenes that exhibit reversible electrochemistry inspired a second generation of dye designs, incorporating both the azulene-thiophene-cyanoacrylic acid D-π-A motif in dyes **19** and **20**, and also the C3 substituents of **40** and **41**. It was hoped that such dyes would display fully reversible electrochemistry, whilst at the same time retaining the D-π-A motif and hence favouring electron injection from the excited state. The second generation target dyes **42**–**44** are shown in Fig. 8.

Of the dye targets **42**–**44**, we first sought to synthesise **42**, bearing a *tert*-butyl group. 1,3-Di-*tert*-butylazulene (**40**, R = R*2* = H) can be synthesised directly from azulene by means of a double Friedel–Crafts alkylation, using excess *tert*-butanol and HBF_4.[74] However, attempts to use this procedure to introduce a *tert*-butyl group directly onto the C3 position of aldehyde **32** were unsuccessful, most likely because the functionality present in this

Table 2
First generation dyes' electrochemical data in THF (E/V vs. Fc/Fc^+).

Dye	E_{pa1} mV	I_{pa1} μA	E_{pa2} mV	I_{pa2} μA	E_{ox} mV	HOMO V vs NHE
Az-1-caa (**3**)	837	18.04	–	–	670	1.30
Az-1-tcaa (**19**)	455	15.79	–	–	310	0.94
TMAz-1-tcaa (**20**)	455	9.22	566	8.88	320	0.95

precursor to dye **19** was incompatible with the harsh Friedel–Crafts reaction conditions. Instead, therefore, we opted to synthesise **42** via a reaction sequence analogous to that for **19**, but starting with 1-*tert*-butylazulene **45** (i.e. a synthesis with the *tert*-butyl group present from the beginning). However, accessing pure 1-*tert*-butylazulene (**45**) is not straightforward. Treatment of azulene with only one equivalent of *tert*-butanol and HBF_4 unavoidably leads to over-substitution, *i.e.* formation of some 1,3-di-*tert*-butylazulene (**40**, $R = R^2 = H$) in addition to the desired 1-*tert*-butylazulene (**45**); in our hands these two products proved to be difficult to separate by chromatography. To overcome this problem, we devised a new synthesis of 1-*tert*-butylazulene. It is known that 1,3-di-*tert*-butylazulene (**40**, $R = R^2 = H$) undergoes *ipso* substitution upon exposure to Vilsmeier conditions, giving 1-formyl-3-*tert*-butylazulene.[75] Furthermore, there are reported examples of 1-formylazulenes undergoing deformylation upon treatment with pyrrole.[76,77] Exploiting these literature reports, we were able to synthesise pure 1-*tert*-butylazulene (**45**) as shown in Scheme 4. Double Friedel–Crafts alkylation of azulene gives 1,3-di-*tert*-butylazulene, which then undergoes substitution of a *tert*-butyl group for a formyl group to give **46**, as per the literature procedures.[74,75] Application of the pyrrole-mediated azulene deformylation protocol to **46** has not been reported previously, but in the event proceeded smoothly to give the desired **45**.

With a reliable route to **45** established, we utilised our sulfonium salt cross-coupling methodology to elaborate this towards dye target **42**. Treatment of **45** with tetramethylenesulfoxide **47** and trifluoroacetic anhydride led to azulenesulfonium salt **48** (after anion exchange). This in turn underwent Suzuki–Miyaura cross-coupling followed by acetal deprotection to give aldehyde **50** (the *tert*-butyl analogue of **32**), as per our reported procedure[68] (Scheme 5).

To synthesise methylthio-substituted dyes **43**–**44**, we were able to employ a more convergent route, introducing the desired –SMe substituent directly onto the azulene 3-position of thienyl aldehydes **32** and **37**, that we had prepared previously. According to the procedure of Shoji, Morita and co-workers, exposure of an azulene to a sulfoxide and an activating agent leads to formation of an azulenesulfonium salt.[78] In many instances, trifluoroacetic anhydride (TFAA) will suffice as the activating agent, but for more electron-poor azulenes (or unactivated arenes[79]), trifluoromethanesulfonic anhydride (Tf_2O) is used. Thus, as shown in Scheme 6, the most nucleophilic position in azulenes **32** and **37** is still the azulene C3 position, regardless of the presence of the thiophene, and it is this position that reacts with the activated sulfoxide to give azulenesulfonium salts **51**–**52**. Whereas we have exploited azulenesulfonium salts for cross coupling (*c.f.* Schemes 2 and 5), Shoji, Morita and co-workers have demonstrated that they may be readily dealkylated to give the corresponding thioethers. In our case, **51** and **52** were not purified, but were instead directly subjected to demethylation conditions to furnish the desired aldehydes **53** and **54**.

With aldehydes **50**, **53** and **54** in hand, access to target dyes **42**–**44** required only the final Knoevenagel condensation with cyanoacrylic acid. Application of the Knoevenagel conditions employed for the first-generation dyes (catalytic piperidine, reflux in acetonitrile) did lead to formation of the target dyes, but the presence of appreciable amounts of residual starting material and other products hampered their purification. The first generation dyes were purified in a straightforward fashion by trituration with dichloromethane, followed by recrystallization, but this protocol was not applicable to the second generation dyes – their greater solubility in dichloromethane precluded effective trituration, and direct recrystallization of the crude was not successful. We therefore sought to improve the Knoevenagel condensation to drive the reaction to completion and reduce the proportion of impurities present in the crude that were interfering with recrystallization. Aside from piperidine, many other promoters of the Knoevenagel reaction have been reported in the literature. Of various literature procedures we tried, use of a stoichiometric quantity of 6-aminocaproic acid in place of piperidine was most beneficial.[80,81] Thus, after optimisation, we found that treatment of **50** with 1 equivalent of 6-aminocaproic acid and 1.5 equivalents of cyanoacrylic acid, in ethanol at 50 °C, led to consumption of starting material by TLC after 3.5 h. Addition of 1 M $H_2SO_{4(aq)}$ then gave a tar, which was dissolved in dichloromethane and washed with water; removal of solvent was followed by a successful recrystallization to give target dye **42** in 49% yield. The same procedure, when applied to **53** and **54** gave a precipitate upon addition of acid, which could simply be isolated by filtration and recrystallized to provide **43** (67% yield) and **44** (63% yield) respectively, as shown in Scheme 7.

With the target second generation dyes **42**–**44** in hand, these were characterised by the same techniques employed for **3**, **19** and **20**. UV–Vis spectra were acquired at 0.01, 0.03 and 0.05 mM concentrations. During the dye synthesis and purification steps, it had been noted that the colour of the dyes in solution differed slightly depending on the solvent used (solvatochromism). When in dichloromethane solution, for instance, the dyes appeared to be somewhat bluer than when acetonitrile was used. Spectra were therefore acquired in three solvents: acetonitrile (MeCN), tetrahydrofuran (THF) and dichloromethane (DCM) (see ESI, Figs. S8–S19). The UV–Vis data for the 2nd generation dyes are presented in Table 3.

The three 2nd generation dyes all have two principal absorption bands in the region of interest, one in the visible region with $\lambda_{max} \approx 430$–$520$ nm (band A) and the other in the near UV with $\lambda_{max} \approx 350$–$380$ nm (band B). Dye MeTTMAz-1-tcaa (**44**) has an additional absorption band with $\lambda_{max} \approx 320$ nm. The band A absorption is assumed to be due to charge transfer between the thiophene linker and the azulene moiety. With dyes tBuAz-1-tcaa (**42**) and MeTAz-1-tcaa (**43**) (*i.e.* those with an unsubstituted azulene 7-membered ring), the absorption band A is the more intense of the two. However, with dye MeTTMAz-1-tcaa (**44**), the situation is reversed, with the absorption band A being less intense than the absorption band B. Indeed, absorption band A for MeTTMAz-1-tcaa (**44**) is only around half the intensity of absorption band A for MeTAz-1-tcaa (**43**). This is an unexpected result at first glance, since the only difference between these two dyes is the presence of the

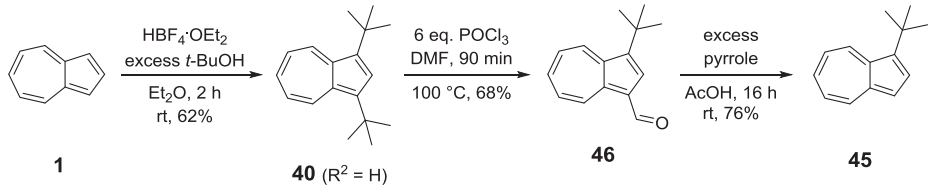

Scheme 4. New synthesis of 1-*tert*-butylazulene.

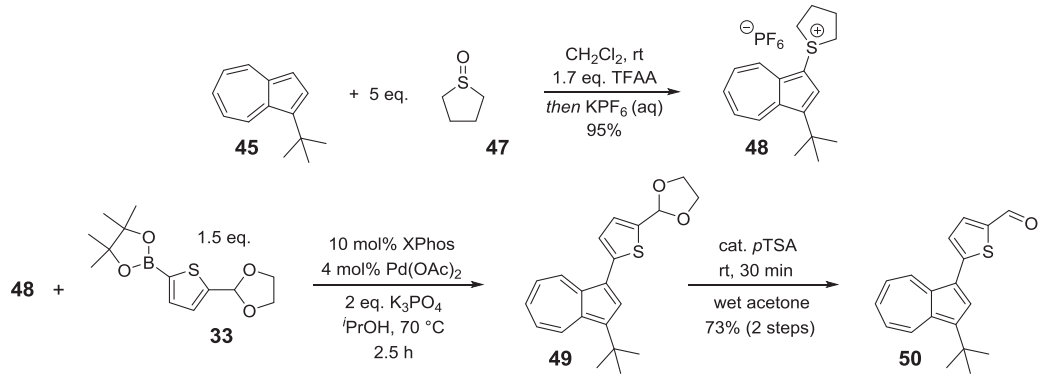

Scheme 5. Synthesis of aldehyde **50**, precursor to dye **42**.

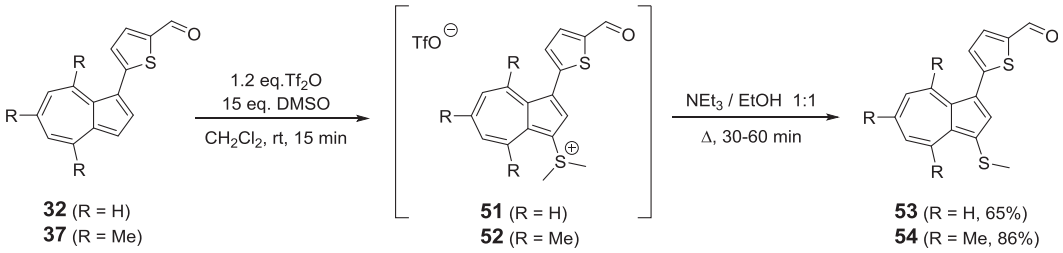

Scheme 6. Direct late-stage C3-functionalisation of thienyl aldehydes.

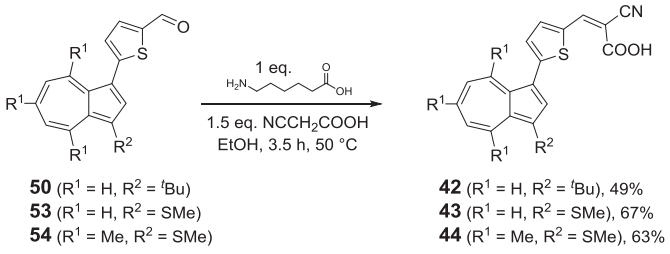

Scheme 7. Final Knoevenagel condensations to produce second generation dyes.

additional methyl groups in **44**, which do not extend the chromophore. Upon reinspection of the UV–vis data for the first generation dyes, the same effect can be discerned. The visible-region absorption band for TMAz-1-tcaa (**20**) is significantly less intense than for Az-1-tcaa (**19**). Once again, the only difference in structure is the presence of the additional methyl groups in **20**.

A possible explanation for the phenomena described above may be found in x-ray crystallographic data acquired for the dyes. Crystals suitable for x-ray diffraction were grown for dyes **20**, **42** and **43**. The structures are depicted in Figs. 9–11.

In the case of MeTAz-1-tcaa (**43**), the structure is essentially planar (Fig. 11), with a torsion angle between the azulene and thiophene rings (defined as Az(C2)-Az(C1)-Thio(C2)-Thio(C3)) of $\theta = 0.9\ (4)^{\circ}$. As such, it seems optimal orbital overlap is achievable in the solid state (and presumably also in solution) and the two rings are fully conjugated. In the case of tBuAz-1-tcaa (**42**), the solid-state structure exhibits some distortion away from planarity (Fig. 10), with the analogous torsion angle being $\theta = 26.8\ (3)^{\circ}$. However, most strikingly of all, in the case of TMAz-1-tcaa (**20**) the

Table 3
UV/Vis data for 2nd generation dyes. Extinction coefficients quoted are mean values of the coefficients calculated for the three dye concentrations.

Dye	Solvent	λ_{max} nm	ε (λ_{max}) L mol^{-1} cm^{-1}	λ_{onset} nm	E_g (opt) eV
tBuAz-1-tcaa (**42**)	MeCN	A: 488	4.12×10^4	567	2.19
		B: 351	2.06×10^4		
	THF	A: 487	3.57×10^4	556	2.23
		B: 353	1.57×10^4		
	DCM	A: 512	3.97×10^4	586	2.12
		B: 358	1.68×10^4		
MeTAz-1-tcaa (**43**)	MeCN	A: 436	1.99×10^4	515	2.41
		B: 357	1.57×10^4		
	THF	A: 478	2.57×10^4	563	2.20
		B: 357	1.52×10^4		
	DCM	A: 497	2.56×10^4	592	2.09
		B: 363	1.43×10^4		
MeTTMAz-1-tcaa (**44**)	MeCN	A: 482	1.15×10^4	597	2.08
		B: 367	2.47×10^4		
	THF	A: 475	1.15×10^4	585	2.12
		B: 362	2.63×10^4		
	DCM	A: 506	1.13×10^4	628	1.97
		B: 377	2.62×10^4		

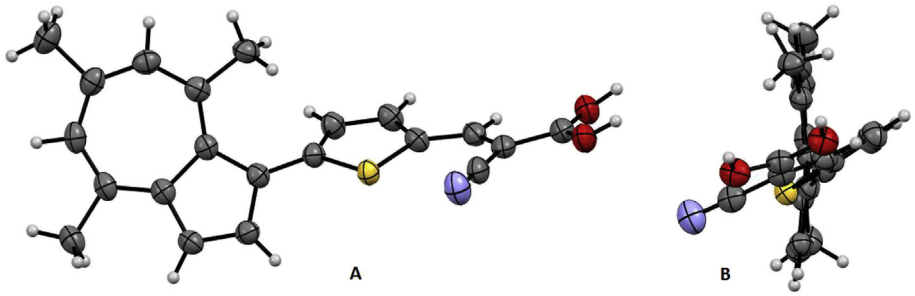

Fig. 9. (A) ORTEP structure of TMAz-1-tcaa (**20**) and (B) rotated through 90° in the horizontal plane to show the "end elevation" view. Ellipsoids are represented at 50% probability. H atoms are shown as spheres of arbitrary radius. CCDC #1815403.

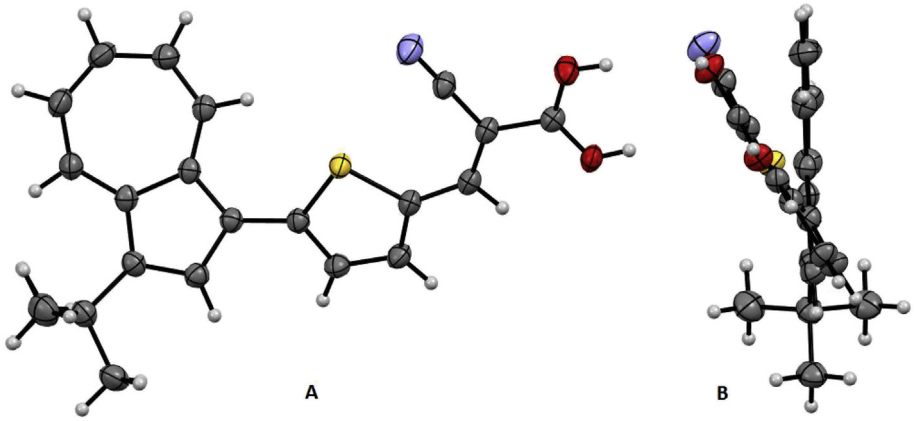

Fig. 10. (A) ORTEP structure of tBuAz-1-tcaa (**42**) and (B) rotated through 90° in the horizontal plane to show the "end elevation" view. Ellipsoids are represented at 50% probability. H atoms are shown as spheres of arbitrary radius. CCDC #1815402.

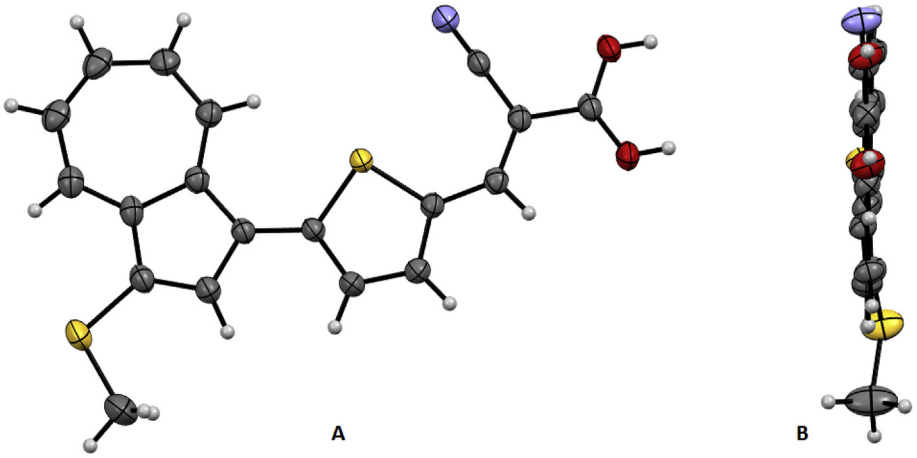

Fig. 11. (A) ORTEP structure of MeTAz-1-tcaa (**43**) and (B) rotated through 90° in the horizontal plane to show the "end elevation" view. Ellipsoids are represented at 50% probability. H atoms are shown as spheres of arbitrary radius. CCDC #1815401.

structure is far from planar (Fig. 9), with the analogous torsion angle being $\theta = 122.2\ (3)^{\circ}$, i.e. the azulene and thiophene rings are closer to being perpendicular than they are to being coplanar. Rather than this being due to any crystal packing effects, we propose this is an unavoidable consequence of the presence of the methyl groups on the azulene 7-membered ring. Thus, if the azulene and thiophene rings were coplanar, the azulene 8-position methyl substituent would be significantly occluded with the thiophene C3 hydrogen. Relief of steric strain therefore necessitates that the thiophene ring rotates out of planarity with the azulene, which will impair the conjugation of the two rings. Since the visible region absorption band is proposed to arise from charge transfer between the azulene and thiophene rings for these dyes, the reduced π-orbital overlap between these two motifs may therefore explain the relatively lower extinction coefficient observed for TMAz-1-tcaa (**20**) in comparison with the analogue Az-1-tcaa (**19**) which lacks the methyl groups. In the case of MeTTMAz-1-tcaa (**44**), although we were not able to obtain an x-ray crystal structure, we can nevertheless propose that the same effect is in operation, leading to the less intense absorption in the visible region

with respect to MeTAz-1-tcaa (**43**) that lacks the methyl groups (and which can be seen in Fig. 11 to be fully planar).

Cyclic voltammograms (CVs) were acquired for the three 2nd generation dyes **42**–**44**. All three dyes show quasi-reversible redox chemistry (Figs. 12–14). The radical cations produced by dye molecule oxidation clearly survive to be reduced back to the dye molecules as evidenced by the reduction waves in the reverse sweep which correspond to the oxidation waves in the forward sweep of the CVs. There is no sign of any decomposition products evident in the second and subsequent scans. For all three dyes, the second and subsequent CV scans are almost exactly super-imposed (scan 1 and scan 3 are plotted for each dye), which indicates that there is little or no depletion of the dye species in the vicinity of the working electrode. This is in contrast with the first generation dye analogues (Figs. 4–6), where the magnitude of the oxidation waves diminish with each successive scan indicating that the dyes are being consumed.

Both of the radical shielding groups therefore appear to do a good job of protecting the radical cation formed by abstracting an electron from the dye molecules. The CVs of the dyes containing a methylthio group (MeTAz-1-tcaa **43** and MeTTMAz-1-tcaa **44**) are very similar; the three methyl groups attached to the 7-membered ring increase the dye oxidation potential by approximately 30 mV. The difference between the methylthio and *tert*-butyl shielding groups is more striking; the shift in oxidation potential between MeTAz-1-tcaa (**43**) and tBuAz-1-tcaa (**42**) is over 250 mV, showing that the dye HOMO energy level can be 'tuned' to a certain extent by changing the shielding group. Electrochemical data extracted from the cyclic voltammograms are presented in Table 4. In the ideal case of a reversible one electron redox couple, the difference between the peak cathodic and anodic potentials (E_{pc} and E_{pa}), ΔE_p is approximately 59 mV (at 25 °C) and the ratio of the peak anodic and cathodic currents (I_{pa} and I_{pc}) is unity.[82] The three dyes depart slightly from this ideal; $\Delta E_p = 131$ mV for all three dyes and I_{pc}/I_{pa} varies from 0.92 to 0.94. It is interesting to note that the values for ΔE_p are identical for each dye, suggesting that the slower than ideal electrode dynamics may be due to a different factor, *e.g.* solvent or electrolyte, which were constant for each experiment.

Energy level data for the first and second generation dyes are summarised in Table 5. The ground state (D^0/D^+) potentials and band gap (E_g) values are taken from the electrochemistry and UV/Vis spectrometry results (see above). Subtracting E_g from D^0/D^+ gives the ground state HOMO level. All of the dyes satisfy the energy level requirements to function as DSSC sensitizers. The redox potential of the ground state is 0.44–0.70 V below that of the I^-/I_3^- couple used in the electrolyte.

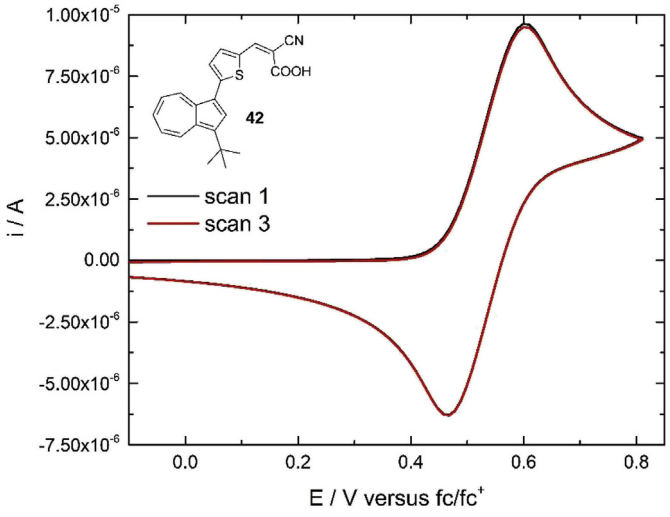

Fig. 12. Voltammogram for tBuAz-1-tcaa (**42**), 0.5 mM in THF. Supporting electrolyte 0.1 M Bu_4NPF_6. Scan rate 100 mV s^{-1}.

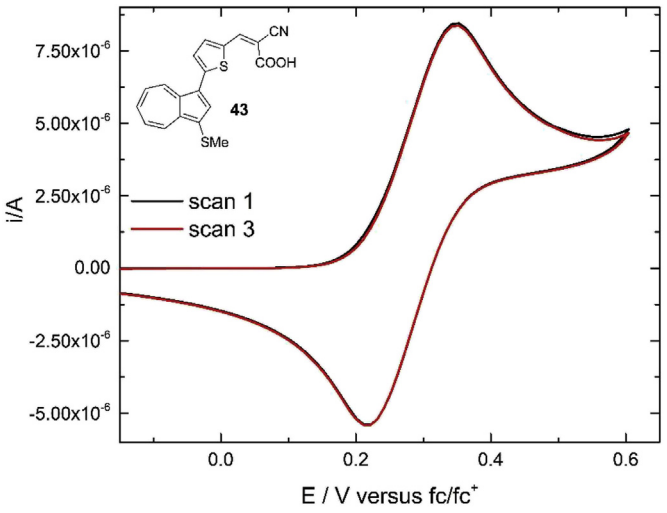

Fig. 13. Voltammogram for MeTAz-1-tcaa (**43**), 0.5 mM in THF. Supporting electrolyte 0.1 M Bu_4NPF_6. Scan rate 100 mV s^{-1}.

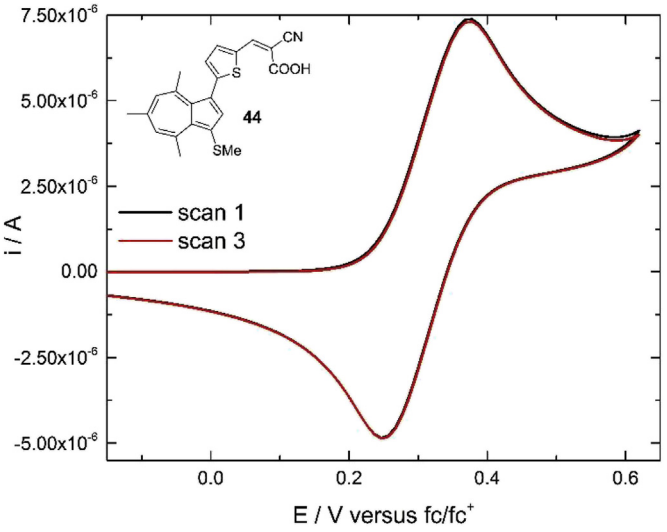

Fig. 14. Voltammogram for MeTTMAz-1-tcaa (**44**), 0.5 mM in THF. Supporting electrolyte 0.1 M Bu_4NPF_6. Scan rate 100 mV s^{-1}.

Construction and evaluation of DSSCs using the first and second generation dyes was then undertaken. The iodide/triiodide redox couple was used, with a 1 cm^2 cell area. Initial experiments with **44** indicated that addition of lithium iodide[83,84] and chenodeoxycholic acid (CA)[85,86] to the electrolyte were both beneficial. Thus, for comparison of all the dyes, the electrolyte composition shown in Table 6 was used. Cells constructed concurrently using dye N719 were also evaluated as a reference for comparison.[5]

The DSSC evaluation results are presented in Table 7 (and graphically in Figs. S20–S23, see ESI). The best result was achieved with the reference dye N719; of our dyes, the highest mean efficiency of 1.20% was achieved with the first generation dye TMAz-1-tcaa (**20**). The next highest performing cells were based on the second generation dye MeTTMAz-1-tcaa (**44**). It is interesting to note that, contrary to expectation, the best performing dyes were

Table 4
Second generation dyes' electrochemical data in THF (E/V vs. Fc/Fc^+).

Dye	E_{pa} mV	E_{pc} mV	ΔE_p mV	$E^0_{½}$ mV	I_{pa} μA	I_{pc} μA	$\frac{I_{pc}}{I_{pa}}$	E_{ox} mV
tBuAz-1-tcaa (**42**)	599	468	131	534	9.63	9.10	0.92	470
MeTAz-1-tcaa (**43**)	352	221	131	287	8.45	7.72	0.92	210
MeTTMAz-1-tcaa (**44**)	378	247	131	312	7.38	6.95	0.94	240

Table 5
First and second generation dyes' energy levels.

Dye	$\frac{D^0}{D^+}$	V vs NHE	E_g (opt) eV	HOMO V vs NHE
Az-1-tcaa (**19**)	0.94		2.27	−1.33
TMAz-1-tcaa (**20**)	0.95		2.27	−1.32
tBuAz-1-tcaa (**42**)	1.1		2.23	−1.13
MeTAz-1-tcaa (**43**)	0.84		2.20	−1.36
MeTTMAz-1-tcaa (**44**)	0.87		2.12	−1.25

Table 6
DSSC electrolyte formulation in acetonitrile.

Component	Concentration
Iodine	0.05 M
1-methyl-3-propyl-imidazonium iodide (ionic liquid)	0.60 M
Lithium Iodide	0.10 M
Chenodeoxycholic acid	0.10 M

the ones based on 4,6,8-trimethylazulene (**25**) and therefore had a methyl group in the seven-membered ring that causes a large torsional angle between the plane of the azulene rings and the thiophene ring of the linker group (see above). This was expected to disrupt conjugation between the azulene and thiophene rings and therefore restrict charge transfer between them too, limiting DSSC performance. However, another factor that detrimentally influences DSSC efficiency is re-combination of electrons injected into the TiO_2 with the oxidised dye species. The high torsional angle of the dyes based on 4,6,8-trimethylazulene may conceivably be beneficial in this respect, helping to block charge transfer from TiO_2 to the oxidised azulene moiety, resulting in improved efficiency.

Two dyes were selected for a more detailed electrolyte additive analysis: first generation dye TMAz-1-tcaa (**20**) and second generation dye tBuAz-1-tcaa (**42**). The three additives to be evaluated in combination were lithium iodide (LiI), chenodeoxycholic acid (CA), and guanidine thiocyanate (GT). GT has been shown to increase DSSC short circuit current density (J_{SC}) and therefore increase efficiency.[87] The DSSC evaluation results for these modified electrolytes are presented in Table 8 (and graphically in Figs. S24–S27, see ESI). The best DSSC efficiencies for both dyes were obtained with the combination of both LiI and CA. As before, the first generation dye TMAz-1-tcaa (**20**) produced the highest efficiency of 1.33% while the second generation dye tBuAz-1-tcaa (**42**) gave an efficiency of 0.92%. The addition of guanidine thiocyanate to the DSSC electrolyte actually had a detrimental effect, reducing DSSC efficiency by 25–33%. Rather than increase short circuit current density, the J_{SC} was severely reduced while open circuit voltage was increased. The addition of LiI and/or CA to the electrolyte both have a positive influence on cell efficiencies and seem to exhibit a synergistic effect when both are added together. The LiI and CA acid both influence the DSSC efficiencies by increasing the closed circuit current density (J_{SC}). While both also reduce the open circuit voltage (V_{OC}), the effect on efficiencies is more than offset by the increased J_{SC}.

Table 7
DSSC cell parameters, with LiI and CA. FF = Fill factor.

Dye	V_{oc} (V)	J_{sc} (mA)	FF (%)	η (%)	η/η_{N719} (%)
N719	0.549	16.07	55.7	4.96	*n/a*
Az-1-tcaa (**19**)	0.309	3.01	61.0	0.57	11.5
	0.311	3.15	59.3	0.59	11.9
	0.305	2.98	54.8	0.50	10.1
Mean	*0.308*	*3.05*	*58.4*	*0.55*	*11.1*
TMAz-1-tcaa (**20**)	0.387	5.38	60.3	1.27	25.6
	0.378	5.17	61.0	1.21	24.3
	0.366	5.07	60.1	1.13	22.8
Mean	*0.377*	*5.21*	*60.5*	*1.20*	*24.2*
tBuAz-1-tcaa (**42**)	0.303	3.06	61.0	0.57	11.5
	0.310	2.54	60.7	0.48	9.7
	0.325	3.11	61.7	0.63	12.7
Mean	*0.313*	*2.90*	*61.1*	*0.56*	*11.3*
MeTAz-1-tcaa (**43**)	0.256	1.71	52.0	0.23	4.6
	0.254	1.78	51.1	0.23	4.6
	0.245	1.80	48.5	0.22	4.4
Mean	*0.252*	*1.76*	*50.5*	*0.23*	*4.6*
MeTTMAz-1-tcaa (**44**)	0.350	3.38	62.3	0.75	15.1
	0.342	3.61	60.8	0.76	15.3
	0.335	3.29	59.1	0.66	13.3
Mean	*0.342*	*3.43*	*60.7*	*0.72*	*14.5*

Table 8
DSSC cell parameters – evaluation of electrolyte additives. FF = Fill factor.

Dye	Additive	V_{oc} (V)	J_{sc} (mA)	FF (%)	η (%)
TMAz-1-tcaa (**20**)	Li	0.498	1.55	71.8	0.56
		0.503	1.40	73.0	0.51
	Mean	*0.501*	*1.48*	*72.4*	*0.54*
	CA, Li	0.391	5.72	59.3	1.33
		0.390	5.73	58.6	1.32
	Mean	*0.391*	*5.73*	*59.0*	*1.33*
	CA, GT	0.544	1.22	75.7	0.50
		0.554	1.37	75.6	0.58
	Mean	*0.549*	*1.30*	*75.7*	*0.54*
	CA, Li, GT	0.482	2.97	69.1	0.99
		0.474	3.00	69.5	0.99
	Mean	*0.478*	*2.99*	*69.3*	*0.99*
tBuAz-1-tcaa (**42**)	Li	0.479	1.11	73.6	0.39
		0.494	1.31	73.4	0.47
	Mean	*0.487*	*1.21*	*73.5*	*0.43*
	CA, Li	0.370	4.14	58.1	0.89
		0.372	4.35	58.1	0.94
	Mean	*0.371*	*4.25*	*58.1*	*0.92*
	CA, GT	0.524	0.94	74.4	0.37
		0.495	0.88	68.1	0.30
	Mean	*0.510*	*0.91*	*71.3*	*0.34*
	CA, Li, GT	0.442	1.89	70.7	0.59
		0.447	2.05	69.1	0.63
	Mean	*0.445*	*1.97*	*69.9*	*0.61*

3. Conclusions

In summary, we have prepared five new azulene-containing dyes and evaluated their performance as sensitizers of titania in dye-sensitized solar cells. The synthesis of these dyes showcases the utility of the azulenesulfonium salt cross-coupling reaction that we have developed, with the dyes being accessed in only 4–5 steps from the parent azulene starting materials. The first generation of dyes (Az-1-tcaa **19** and TMAz-1-tcaa **20**) were shown by cyclic

voltammetry to display non-reversible electrochemistry. This in turn prompted a literature search for azulenes that are known to exhibit reversible electrochemistry. Based on the results of this search, second generation dyes were rationally designed to target the desired property of reversible electrochemistry. The second generation dyes (tBuAz-1-tcaa **42**, MeTAz-1-tcaa **43** and MeTTMAz-1-tcaa **44**) were synthesised and it was shown by cyclic voltammetry that they do indeed exhibit reversible electrochemistry. However, when both the first and second generation dyes were evaluated in dye-sensitized solar cells, no trend for increased efficiency of the second generation dyes over the first generation dyes was observed. This implies that stability of the oxidised form of the dye was not the dominant factor in determining overall cell efficiency; we instead propose a rationale for the observed efficiencies based on an increased torsional angle between the azulene and thiophene rings induced by the presence of the additional methyl substituents in dyes **20** and **44** (the two dyes with highest η).

Acknowledgements

We thank the University of Bath (for a PhD fee waiver to Paul Cowper) and EPSRC (CDT PhD studentship for Adam Pockett, Grant EP/G03768X/1).

Appendix A. Supplementary data

Supplementary data related to this article can be found at https://doi.org/10.1016/j.tet.2018.04.043.

References

1. Tian H, Huang S, Zhou C. *Acta Phys - Chim Sin*. 1988;4:314–319.
2. O'Regan B, Grätzel M. *Nature*. 1991;353:737–740.
3. Hagfeldt A, Boschloo G, Sun L, Kloo L, Pettersson H. *Chem Rev*. 2010;110:6595–6663.
4. Hardin BE, Snaith HJ, McGehee MD. *Nat Photon*. 2012;6:162–169.
5. Nazeeruddin Md K, Zakeeruddin SM, Humphry-Baker R, et al. *Inorg Chem*. 1999;38:6298–6305.
6. Amaresh M, Markus KR, Bäuerle P. *Angew Chem Int Ed*. 2009;48:2474–2499.
7. Kim B-G, Chung K, Kim J. *Chem Eur J*. 2013;19:5220–5230.
8. Liang M, Chen J. *Chem Soc Rev*. 2013;42:3453–3488.
9. Wang J, Liu K, Ma L, Zhan X. *Chem Rev*. 2016;116:14675–14725.
10. Li X, Zhang X, Hua J, Tian H. *Mol Syst Des Eng*. 2017;2:98–122.
11. Kumaresan P, Vegiraju S, Ezhumalai Y, et al. *Polymers*. 2014;6:2645–2669.
12. Wills KA, Mandujano-Ramirez HJ, Merino G, et al. *Dyes Pigments*. 2016;134:419–426.
13. Wang Z-S, Koumura N, Cui Y, et al. *Chem Mater*. 2008;20:3993–4003.
14. Li G, Jiang K-J, Li Y-F, Li S-L, Yang L-M. *J Phys Chem C*. 2008;112:11591–11599.
15. Hua Y, Chang S, He J, et al. *Chem Eur J*. 2014;20:6300–6308.
16. Hung W-I, Liao Y-Y, Hsu C-Y, et al. *Chem Asian J*. 2014;9:357–366.
17. Kalyanasundaram K, Grätzel M. *Coord Chem Rev*. 1998;177:347–414.
18. Polo AS, Itokazu MK, Iha NYM. *Coord Chem Rev*. 2004;248:1343–1361.
19. Kurotobi K, Kim KS, Noh SB, Kim D, Osuka A. *Angew Chem Int Ed*. 2006;45:3944–3947.
20. Muranaka A, Yonehara M, Uchiyama M. *J Am Chem Soc*. 2010;132:7844–7845.
21. Oda M, Thanh NC, Ikai M, Fujikawa H, Nakajima K, Kuroda S. *Tetrahedron*. 2007;63:10608–10614.
22. Thanh NC, Ikai M, Kajioka T, et al. *Tetrahedron*. 2006;62:11227–11239.
23. Koch M, Blacque O, Venkatesan K. *Org Lett*. 2012;14:1580–1583.
24. Koch M, Blacque O, Venkatesan K. *J Mater Chem C*. 2013;1:7400–7408.
25. Murai M, Iba S, Ota H, Takai K. *Org Lett*. 2017;19:5585–5588.
26. Ito S, Morita N. *Eur J Org Chem*. 2009:4567–4579.
27. Yamaguchi Y, Takubo M, Ogawa K, Nakayama K-I, Koganezawa T, Katagiri H. *J Am Chem Soc*. 2016;138:11335–11343.
28. Yamaguchi Y, Ogawa K, Nakayama K-I, Ohba Y, Katagiri H. *J Am Chem Soc*. 2013;135:19095–19098.
29. Wang F, Lai Y-H, Kocherginsky NM, Kosteski YY. *Org Lett*. 2003;5:995–998.
30. Cristian L, Sasaki I, Lacroix PG, et al. *Chem Mater*. 2004;16:3543–3551.
31. Lopez-Alled CM, Sanchez-Fernandez A, Edler KJ, et al. *Chem Commun*. 2017;53:12580–12583.
32. Xin H, Gao X. *ChemPlusChem*. 2017;82:945–956.
33. Dong J-X, Zhang H-L. *Chin Chem Lett*. 2016;27:1097–1104.
34. Ramadan M, Goeters S, Watzer B, et al. *J Nat Prod*. 2006;69:1041–1045.
35. Rekka E, Chrysselis M, Siskou I, Kourounakis A. *Chem Pharm Bull*. 2002;50:904–907.
36. Zhang L-Y, Yang F, Shi W-Q, Zhang P, Li Y, Yin S-F. *Bioorg Med Chem Lett*. 2011;21:5722–5725.
37. Yanagisawa T, Kosakai K, Tomiyama T, Yasunami M, Takase K. *Chem Pharm Bull*. 1990;38:3355–3358.
38. Yanagisawa T, Wakabayashi S, Tomiyama T, Yasunami M, Takase K. *Chem Pharm Bull*. 1988;36:641–647.
39. Sekine T, Takahashi J, Nishishiro M, et al. *Anticancer Res*. 2007;27:133–144.
40. Wakabayashi H, Hashiba K, Yokoyama K, et al. *Anticancer Res*. 2003;23:4747–4755.
41. Asato AE, Peng A, Hossain MZ, Mirzadegan T, Bertram JS. *J Med Chem*. 1993;36:3137–3147.
42. Ishihara M, Wakabayashi H, Motohashi N, Sakagami H. *Anticancer Res*. 2011;31:515–520.
43. Peet J, Selyutina A, Bredihhin A. *Bioorg Med Chem*. 2016;24:1653–1657.
44. Liu RSHJ. *Chem Educ*. 2002;79:183–185.
45. Liu RSH, Asato AE. *J Photochem Photobiol C*. 2003;4:179–194.
46. Puodziukynaite E, Wang H-W, Lawrence J, et al. *J Am Chem Soc*. 2014;136:11043–11049.
47. Umeyama T, Watanabe Y, Miyata T, Imahori H. *Chem Lett*. 2015;44:47–49.
48. Yao J, Cai Z, Liu Z, et al. *Macromolecules*. 2015;48:2039–2047.
49. Xin H, Ge C, Jiao X, et al. *Angew Chem Int Ed*. 2018;57:1322–1326.
50. Chen Y, Zhu Y, Yang D, et al. *Chem Eur J*. 2016;22:14527–14530.
51. Ince M, Bartelmess J, Kiessling D, et al. *Chem Sci*. 2012;3:1472–1480.
52. Nishimura H, Ishida N, Shimazaki A, et al. *J Am Chem Soc*. 2015;137:15656–15659.
53. Pagba C, Zordan G, Galoppini E, et al. *J Am Chem Soc*. 2004;126:9888–9889.
54. Lamberto M, Pagba C, Piotrowiak P, Galoppini E. *Tetrahedron Lett*. 2005;46:4895–4899.
55. Zhang X-H, Li C, Wang W-B, Cheng X-X, Wang X-S, Zhang B-W. *J Mater Chem*. 2007;17:642–649.
56. Kakiage K, Fujimura E, Nakada Y, Ogino T, Kyomen T, Hanaya M. *Key Eng Mater*. 2014;596:35–39. https://doi.org/10.4028/www.scientific.net/KEM.596.35.
57. Tanabe J, Shinkai M, Tsuchiya M. Japanese patent, 2008. JP 2008101063 (A).
58. Tanabe J, Shinkai M, Tsuchiya M. Japanese patent, 2008. JP 2008101065 (A).
59. Braun MJ, Gutmann S, Woehrle D, Miyaji T. *Eur Pat Appl*. 2014. EP 2700641 A1.
60. Hiraide M, Machida S. Japanese patent, 2016. JP2016134570 (A).
61. Farrand L, Findlater M, Giles M, et al. *Eur Pat Appl*. 2003. EP 1318185 A1.
62. Maggio E, Martsinovich N, Troisi A. *Angew Chem Int Ed*. 2013;52:973–975.
63. Carret S, Blanc A, Coquerel Y, Berthod M, Greene AE, Deprés J-P. *Angew Chem Int Ed*. 2005;44:5130–5133.
64. Walker SD, Barder TE, Martinelli JR, Buchwald SL. *Angew Chem Int Ed*. 2004;43:1871–1876.
65. Fuse S, Sugiyama S, Maitani MM, et al. *Chem Eur J*. 2014;20:10685–10694.
66. Lai L-F, Ho C-L, Chen Y-C, et al. *Dyes Pigments*. 2013;96:516–524.
67. Anderson Jr AG, Nelson JA, Tazuma JJ. *J Am Chem Soc*. 1953;75:4980–4989.
68. Cowper P, Jin Y, Turton MD, Kociok-Köhn G, Lewis SE. *Angew Chem Int Ed*. 2016;55:2564–2568.
69. Razus AC, Nitu C, Tecuceanu V, Cimpeanu V. *Eur J Org Chem*. 2003:4601–4610.
70. Juris A, Balzani V, Barigelletti F, Campagna S, Belser P, von Zelewsky A. *Coord Chem Rev*. 1988;84:85–277.
71. Gerson F, Scholz M, Hansen H-J, Uebelhart P. *J Chem Soc Perkin Trans*. 1995;2:215–220.
72. Shoji T, Ito S, Toyota K, Iwamoto T, Yasunami M, Morita N. *Eur J Org Chem*. 2009:4307–4315.
73. Becker DA, Natero R, Echegoyen L, Lawson RC. *J Chem Soc Perkin Trans*. 1998;2:1289–1291.
74. Hafner K, Stephan A, Bernhardt C. *Liebigs Ann Chem*. 1961;650:42–62.
75. Hafner K, Moritz KL. *Liebigs Ann Chem*. 1962;656:40–53.
76. Ito S, Morita N, Asao T. *Bull Chem Soc Jpn*. 1999;72:2543–2548.
77. Shoji T, Ito S, Okujima T, et al. *Eur J Org Chem*. 2009:1554–1563.
78. Shoji T, Higashi J, Ito S, et al. *Eur J Org Chem*. 2008:1242–1252.
79. Nenajdenko VG, Popov VI, Balenkova ES. *Sulfur Lett*. 1996;20:75–83.
80. Prout FS. *J Org Chem*. 1953;18:928–933.
81. Prout FS, Abel-Latif AA, Kamal MR. *J Chem Eng Data*. 1963;8:597–599.
82. Fisher AC. *Electrode Dynamics*. Oxford University Press; 1996:31–32.
83. Taya S, Kuwahara S, Shen Q, Toyoda T, Katayama K. *RSC Adv*. 2014;4:21517–21520.
84. Bai Y, Zhang J, Wang Y, Zhang M, Wang P. *Langmuir*. 2011;27:4749–4755.
85. Daeneke T, Kwon T-H, Holmes AB, Duffy NW, Bach U, Spiccia L. *Nat Chem*. 2011;3:211–215.
86. Salvatori P, Marotta G, Cinti A, Anselmi C, Mosconi E, De Angelis F. *J Phys Chem C*. 2013;117:3874–3887.
87. Zhang C, Huang Y, Huo Z, Chen S, Dai S. *J Phys Chem C*. 2009;113:21779–21783.